



Topological quantized edge pumping spin flip in the Rice-Mele model with spin-orbit coupling

E. S. Ma  and Z. Song **School of Physics, Nankai University, Tianjin 300071, China*

(Received 23 December 2024; revised 15 April 2025; accepted 22 April 2025; published 5 May 2025)

The quantized Thouless pumping charge in a spinless Rice-Mele model originates from a degeneracy point in the parameter space and cannot be detected when open boundary conditions are applied. In this work, we investigate the topological features of a spinful Rice-Mele model. We demonstrate that spin-orbit coupling facilitates the transition of a single degenerate point into a degenerate loop, which is anticipated to be the source of the topological characteristics. When periodic boundary conditions are considered, we find that the pumping spin is zero for an adiabatic loop within the nodal loop and is 2 (in units of $\hbar/2$) for an adiabatic passage enclosing the nodal loop. When open boundary conditions are considered, the boundary-bulk correspondence is demonstrated by quantized pumping spin flips at the edges, which can be obtained by completing double periods of a closed passage, rather than a single cycle. Our findings reveal an alternative dynamic manifestation of the boundary-bulk correspondence.

DOI: [10.1103/PhysRevB.111.195109](https://doi.org/10.1103/PhysRevB.111.195109)

I. INTRODUCTION

Thouless pumping, as the quantum version of matter pumping [1] by a mechanical device, has garnered significant attention over a long period. It involves the transport of charge without a net external electric or magnetic field, achieved through an adiabatic cyclic evolution of the underlying Hamiltonian. In contrast to transport by a classical device, the transported charge in a Thouless pump exhibits two intriguing features. First, the total probability of the transferred particles is precisely quantized during a cyclic adiabatic passage. Secondly, as a demonstration of topological invariant, a nonzero pumping charge for the ground state is shown to be related to a degenerate point [2]. Recently, the versatility and control of synthetic quantum systems have made experimental realization of quantum pumping possible. Electron pumping experiments have been performed in various semiconductor-based nanoscale devices [3–5]. More recently, the topological charge pump was realized in optical superlattices based on ultracold atom technology [6–8] and it has been also extensively studied in theory [9–17]. To date, there have been many works focusing on the topological pumping charge in different systems, such as in superconducting circuits [18–21], in multi-terminal Josephson junctions of conventional superconductors [22,23], and in topological superconductors [24–28].

In this work, we studied the topological Thouless pumping of a spinful Rice-Mele (RM) chain with spin-orbit coupling. In general, the quantized Thouless pumping charge in a spinless RM model originates from a degeneracy point in the parameter space. We demonstrate that spin-orbit coupling facilitates the transition of a single degenerate point into a degenerate loop, which is anticipated to be the source of the topological characteristics. There has been a

substantial amount of prior work focusing on the topology of the nodal line, primarily in semimetals, such as those reported in [29–33]. Additionally, research has also been conducted on materials with spin-orbit coupling, including [34–37]. It is important to note that, in semimetals, the nodal line is a degeneracy line that lies in three-dimensional momentum space rather than parameter space in our scenario and its topological properties are demonstrated through the integral of the Berry connection in momentum space along a loop that interlocks with the degenerate loop [29,31,32]. When periodic boundary conditions are considered, analytical and numerical studies show that the pumping charge remains zero as the degenerate point transitions to a nodal circle. In contrast, we find that the pumping spin is zero for an adiabatic loop within the nodal loop and is 2 (in units of $\hbar/2$) for an adiabatic passage enclosing the nodal loop. Up to now, topological spin pumping has been extensively studied in numerous works. These studies include theoretical perspectives on systems with spin-orbit interaction [38–45] and experimental realizations in superlattices, superconductors, and magnetic systems [46–48]. The Z_2 invariant [49] and the spin Chern number [50,51] have been proposed to characterize the topological properties determined by symmetry. In addition, we also investigate a dynamic manifestation of the boundary-bulk correspondence. We calculate the pumping spin flip for different adiabatic passages under the open boundary conditions. We find that the quantized pumping spin flips at the edges can be obtained only when double periods of a closed passage are considered. The pumping spin flips at the edges is zero for an adiabatic loop within the nodal loop and is 2 (in units of $\hbar/2$) for an adiabatic passage enclosing the nodal loop. Our findings not only propose an origin for the topology but also provide another method for dynamically detecting the boundary-bulk correspondence. The structure of the paper is outlined as follows. We commence in Sec. II by presenting the Hamiltonian and examining its symmetry. In Sec. III, for a straightforward

*Contact author: songtc@nankai.edu.cn

scenario where spin-orbit coupling is absent, we assess the validity of employing pumping charge as a topological indicator. Consequently, we introduce the concept of topological pumping spin. In Sec. IV, we derive the zero-energy point equation of the energy band in parameter space under periodic boundary conditions. The topological properties of the system originate from this equation. In Sec. V, we focus on the case where spin-orbit coupling is negligible. We theoretically investigate the pumping spin of every energy band using perturbation theory. Furthermore, we present numerical results for the general case of spin-orbit coupling, which demonstrate that the pumping spin is a universal topological invariant for the system. In Sec. VI, we introduce the concepts of spin-flip current and pumping spin flip. Our numerical simulations demonstrate that the distribution of the pumping spin flip exhibits marginal characteristics and the aggregate of the marginal pumping spin flips is found to be quantized. We draw conclusions in Sec. VII. Some detailed derivations are given in the Appendices.

II. MODEL AND SYMMETRY

Considering the one-dimensional RM model on $2N$ lattice with spin-orbit coupling, the Hamiltonian is

$$H = \sum_{\sigma=\uparrow,\downarrow} H_{\sigma} + H_{\text{so}}, \quad (1)$$

where the coupling-free part is

$$H_{\sigma} = \sum_{j=1}^{2N} (-1)^j \left[\frac{1 + (-1)^j \delta}{2} (c_{j,\sigma}^{\dagger} c_{j+1,\sigma} + \text{H.c.}) - (-1)^j V c_{j,\sigma}^{\dagger} c_{j,\sigma} \right] \quad (2)$$

and the spin-orbit coupling term is

$$H_{\text{so}} = \frac{\lambda}{2} \sum_{j=1}^{2N} \sum_{\sigma=\uparrow,\downarrow} [(-1)^{\sigma} c_{j,\sigma}^{\dagger} c_{j+1,-\sigma} + \text{H.c.}] \quad (3)$$

Here, $H_{\uparrow} + H_{\downarrow}$ can be seen as two independent RM models with opposite spin and $c_{j,\sigma}^{\dagger}$ is the fermion creation operator at site j ; $\sigma = \uparrow, \downarrow$ denotes spin polarization. We have $c_{2N+1,\sigma} = c_{1,\sigma}$ for the system with periodic boundary condition, while $c_{2N+1,\sigma} = 0$ for open boundary condition. The strength of hopping is dimensionless and spin-dependent, given by $(-1)^{\uparrow} = -(-1)^{\downarrow} = 1$. Term H_{so} characterizes the spin-orbit coupling with the strength $\lambda/2$.

For the Hamiltonian $H_{\uparrow} + H_{\downarrow}$, both total fermion number n with spin $\sigma = \uparrow, \downarrow$ and total spin component s_z are conservative, that is

$$[n_{\sigma}, H_{\uparrow} + H_{\downarrow}] = [s_z, H_{\uparrow} + H_{\downarrow}] = 0, \quad (4)$$

where

$$n_{\sigma} = \sum_{j=1}^{2N} c_{j,\sigma}^{\dagger} c_{j,\sigma} \quad (5)$$

and

$$s_{\alpha} = \sum_{j=1}^{2N} s_j^{\alpha}. \quad (6)$$

Here the spin operators s^{α} ($\alpha = x, y, z$) at j th site (in units of $\hbar/2$) are defined as

$$s_j^{\alpha} = (c_{j,\uparrow}^{\dagger} \ c_{j,\downarrow}^{\dagger}) \sigma^{\alpha} \begin{pmatrix} c_{j,\uparrow} \\ c_{j,\downarrow} \end{pmatrix}, \quad (7)$$

where σ^{α} ($\alpha = x, y, z$) are Pauli matrices, given as

$$\sigma^x = \begin{pmatrix} 0 & 1 \\ 1 & 0 \end{pmatrix}, \quad \sigma^y = \begin{pmatrix} 0 & -i \\ i & 0 \end{pmatrix}, \quad \sigma^z = \begin{pmatrix} 1 & 0 \\ 0 & -1 \end{pmatrix}. \quad (8)$$

We note that the term H_{so} breaks the conservations of n_{σ} and s_z , but remains the conservation of total fermion number $n = n_{\uparrow} + n_{\downarrow}$. In addition, defining a spin-flipping operator R as follows

$$R c_{j,\sigma} R^{-1} = c_{j,-\sigma}, \quad (9)$$

which flips a spin to the opposite direction, we have

$$R H R^{-1} = -H. \quad (10)$$

This means that the energy levels of H are symmetric with respect to 0. In addition, considering a gauge transformation as follows

$$A c_{j,\sigma} A^{-1} = (-1)^j c_{j,\sigma}, \quad (11)$$

with $j \in [1, 2N]$, then we have

$$R A H(V) (R A)^{-1} = H(-V), \quad (12)$$

which indicates that $H(V)$ and $H(-V)$ have the same spectrum.

III. TOPOLOGICAL PUMPING SPIN

In this work, we investigate the topology of the Hamiltonian H by considering the time-dependent parameter $\delta = \delta(t)$ and $V = V(t)$. To proceed, we first give a brief review of features of the Hamiltonian H_{σ} . It can be diagonalized in the form

$$H_{\sigma} = \sum_k \varepsilon_{k,\sigma} (\alpha_{k,\sigma}^{\dagger} \alpha_{k,\sigma} - \beta_{k,\sigma}^{\dagger} \beta_{k,\sigma}), \quad (13)$$

where the spectrum is given by

$$\varepsilon_{k,\sigma} = \sqrt{V^2 + |\gamma_k|^2}. \quad (14)$$

Here $\gamma_k = [(1 - \delta) + (1 + \delta)e^{ik}]/2$ and wave vector $k = 2n\pi/N$, $n = 1, 2, \dots, N$. Two sets of fermion operators $\{\alpha_{k,\sigma}, \beta_{k,\sigma}\}$ can be extracted from the single-particle solution of the equation, given by

$$H_{\sigma} |\psi_{k,\sigma}^{\pm}\rangle = \pm \varepsilon_{k,\sigma} |\psi_{k,\sigma}^{\pm}\rangle, \quad (15)$$

where $|\psi_{k,\sigma}^{+}\rangle = \alpha_{k,\sigma}^{\dagger} |0\rangle$ and $|\psi_{k,\sigma}^{-}\rangle = \beta_{k,\sigma}^{\dagger} |0\rangle$. Here $|0\rangle$ is the vacuum state satisfying $\alpha_{k,\sigma} |0\rangle = \beta_{k,\sigma} |0\rangle = 0$. For the adiabatic time evolution along an arbitrary loop with

$$\delta(t + T) = \delta(t), \quad V(t + T) = V(t), \quad (16)$$

the pumping charge $Q_\sigma = \int_0^T J_\sigma dt$ is shown to be a demonstration of the Chern number, where the current across two neighboring sites is equivalent to the k integral of the Berry curvature, that is

$$J_\sigma = \frac{i}{2\pi} \int_0^{2\pi} [(\partial_t \langle \psi_{k,\sigma}^- |) \partial_k | \psi_{k,\sigma}^- \rangle - (\partial_k \langle \psi_{k,\sigma}^- |) \partial_t | \psi_{k,\sigma}^- \rangle] dk. \quad (17)$$

We have the following topological characteristics:

$$Q_\sigma = \begin{cases} (-1)^\sigma, & \text{enclosed } (0, 0), \\ 0, & \text{otherwise,} \end{cases} \quad (18)$$

which arise from the degenerate point at $(\delta, V) = (0, 0)$. The pumping charge can be computed by quasiadiabatic passage. Obviously, for the ground state of $H_\uparrow + H_\downarrow$ the obtained pumping charge $Q_\uparrow + Q_\downarrow$ is vanishing whether the loop in the $\delta - V$ plane encloses the origin or not. Then the topological invariant in $H_\uparrow + H_\downarrow$ cannot be detected via the pumping charge.

Nevertheless, it is obvious that the sub-Hamiltonians H_\uparrow and H_\downarrow are really topologically nontrivial. We need an alternative topological invariant to characterize such topology. Technically, an amount of pumping charge Q_σ is always associated with an amount of pumping spin $(-1)^\sigma Q_\sigma$. Then we can employ the total pumping spin for the ground state, defined as $S = Q_\uparrow - Q_\downarrow$, as topologically invariant, which obeys

$$S = \begin{cases} 2, & \text{enclosed } (0, 0), \\ 0, & \text{otherwise.} \end{cases} \quad (19)$$

In the following, we will investigate what happens in the presence of spin-orbit coupling.

IV. NODAL CIRCLE

In this section, we focus on the solution of the system in the presence of spin-orbit coupling. Under periodic boundary conditions, the system has translational symmetry, with each unit cell including four degrees of freedom. Employing Fourier transformation

$$\begin{pmatrix} c_{2j-1,\uparrow} \\ c_{2j,\uparrow} \\ c_{2j-1,\downarrow} \\ c_{2j,\downarrow} \end{pmatrix} = \frac{e^{ikj}}{\sqrt{N}} \begin{pmatrix} a_{k,\uparrow} \\ b_{k,\uparrow} \\ b_{k,\downarrow} \\ a_{k,\downarrow} \end{pmatrix}, \quad (20)$$

the Hamiltonian can be written as

$$H = \sum_{2\pi > k > 0} \Psi_k^\dagger h_k \Psi_k, \quad (21)$$

where the operator vector is defined as

$$\Psi_k^\dagger = (a_{k,\uparrow}^\dagger \quad b_{k,\uparrow}^\dagger \quad a_{k,\downarrow}^\dagger \quad -b_{k,\downarrow}^\dagger) \quad (22)$$

and the core matrix is

$$h_k = \begin{pmatrix} V & \zeta & \xi & 0 \\ \zeta^* & -V & 0 & \xi^* \\ \xi^* & 0 & V & \zeta^* \\ 0 & \xi & \zeta & -V \end{pmatrix}. \quad (23)$$

Here the k -dependent factors are given by

$$\begin{aligned} \zeta &= [1 - \delta + (1 + \delta)e^{-ik}]/2, \\ \xi &= \lambda(1 - e^{-ik})/2. \end{aligned} \quad (24)$$

The four eigenvalues of h_k can be expressed as

$$\varepsilon_{\mu,v} = \mu \sqrt{\zeta \zeta^* + \xi \xi^* + V^2} + v \sqrt{4V^2 \xi \xi^* + (\zeta \xi^* + \xi \zeta^*)^2}, \quad (25)$$

with $\mu, v = \pm$. The derivations in the Appendixes show that the energy gap between positive and negative bands closes only when $k = 0$ or π . The corresponding zero-energy points form a nodal loop in the $\delta - V$ plane, obeying the equation

$$\delta^2 + V^2 = \lambda^2. \quad (26)$$

Obviously, it is a circle with radius λ centered at the origin. In Fig. 1, the spectral structure in the parameter space, obtained from the spectrum $\varepsilon_{\mu,v}$, is plotted for different values of λ as an illustration.

V. TOPOLOGY ORIGINATED FROM NODAL LOOP

It has been shown that the quantized Thouless pumping of charge and spin in the RM model, in the absence of spin-orbit coupling, originates from the degeneracy point at the origin. Furthermore, this is also true when multiple degenerate points are involved. Now, a natural question arises: what happens when these degenerate points form a degenerate loop, which contains an infinite number of degenerate points? Our strategy consists of two steps: (i) we perform an analytical analysis by considering an adiabatic loop that is far from the nodal circle; (ii) we conduct numerical simulations to verify the results obtained.

Now we focus on the first step. The spin-orbit coupling term H_{so} can be regarded as perturbation under the condition $\delta^2 + V^2 \gg \lambda^2$. In the following, we only focus on the negative energy bands. Applying the perturbation method, we can get zero-order approximation eigenstates of h_k for two negative energy bands, given by

$$|\varphi_k^\pm\rangle = \frac{|\psi_{k,\downarrow}^- \rangle \mp \text{sgn}(\lambda) e^{i\Lambda_k} |\psi_{k,\uparrow}^- \rangle}{\sqrt{2}}, \quad (27)$$

where the factor Λ_k is given by

$$\Lambda_k = \arg \left[\sin \left(\phi_k - \frac{k}{2} \right) + i \cos \theta_k \cos \left(\phi_k - \frac{k}{2} \right) \right] - \phi_k, \quad (28)$$

with

$$\begin{aligned} \theta_k &= \arctan \left[\frac{\sqrt{1 + \delta^2 + (1 - \delta^2) \cos k}}{\sqrt{2}V} \right], \\ \phi_k &= \arctan \left[\frac{(1 + \delta) \sin k}{(1 - \delta) + (1 + \delta) \cos k} \right]. \end{aligned} \quad (29)$$

Accordingly, for an adiabatic time evolution along an arbitrary loop far from the nodal loop, the pumping charge for each band is $Q^\pm = \int_0^T J^\pm dt$. Here the current across two

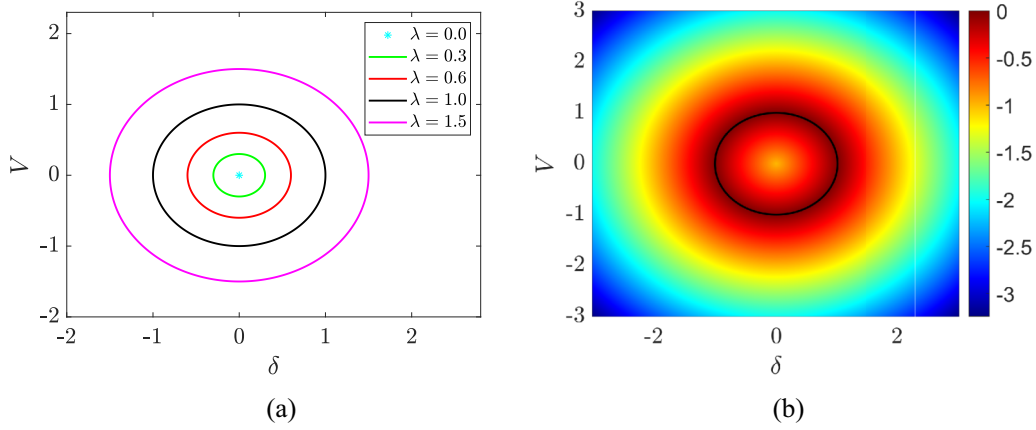


FIG. 1. Spectral structure in the parameter space for the Hamiltonian given by Eq. (1). (a) Several representative nodal circles derived from Eq. (26) on the $\delta - V$ plane for different spin-orbit coupling strengths, as indicated in the panel. (b) Color contour plots of the energy band $\epsilon_{-, -}$ from Eq. (25), with the wave vector k set to π . The black circle represents $\lambda = 1$, which corresponds to the one plotted in (a).

neighboring sites is

$$J^\pm = \frac{i}{2\pi} \int_0^{2\pi} [(\partial_t \langle \varphi_k^\pm |) \partial_k | \varphi_k^\pm \rangle - (\partial_k \langle \varphi_k^\pm |) \partial_t | \varphi_k^\pm \rangle] dk. \quad (30)$$

Since the factor Λ_k has no contribution to the Berry curvature, direct derivations show that

$$J^\pm = \frac{1}{2} (J_\uparrow + J_\downarrow). \quad (31)$$

Then the pumping charge $Q^\pm = (Q_\uparrow + Q_\downarrow)/2$ is vanishing whether the loop in the $\delta - V$ plane encloses the nodal circle or not. In contrast, the pumping spin for the ground state can also be regarded as a topological invariant, obeying

$$S = \begin{cases} 2, & \text{enclosed the nodal circle,} \\ 0, & \text{otherwise.} \end{cases} \quad (32)$$

This conclusion should still hold true when the adiabatic loop approaches the nodal circle due to the fact that the Chern number must be an integer. On the other hand, although the nodal loop is in the two-dimensional parameter space rather than in three-dimensional momentum space as in the semimetal system, we find that, within a certain parameter region, we can map our model to a semimetal model studied in a previous work by adjusting the parameters δ and V . In this previous work [52], a Z_2 invariant defined on a sphere enclosing the whole nodal loop is given and the details are presented in Appendix B. However, it is a challenge for us to establish the correspondence between the quantized spin pumping and the Z_2 invariant. This should be an interesting topic for future work.

Now we turn to the second step. In order to verify and demonstrate the conclusions, numerical simulations are performed for quasiadiabatic time evolution in finite systems. The driven system adopts periodic boundary conditions to simulate the dynamic behavior of the topology originating from the nodal circles. To this end, we introduce the local charge current $\hat{J}_{l,\sigma}$ and spin current \hat{S}_l operators as

$$\hat{J}_{l,\sigma} = \frac{1 + (-1)^l \delta}{2i} (-1)^\sigma c_{l,\sigma}^\dagger c_{l+1,\sigma} + \text{H.c.}, \quad (33)$$

$$\hat{S}_l = \frac{1 + (-1)^l \delta}{2i} \sum_\sigma c_{l,\sigma}^\dagger c_{l+1,\sigma} + \text{H.c.}, \quad (34)$$

for the dimer across two neighboring sites l and $l+1$ with $l \in [1, 2N]$.

In the following we are going to calculate the pumping charge and spin of ground state for a quasiadiabatic passage in the parameter space. We consider the time-dependent Hamiltonian $H(t)$ with periodically varying parameters as follows:

$$\begin{aligned} \delta(t) &= R_1 \cos(\omega t + \theta_0) + \delta_0, \\ V(t) &= R_2 \sin(\omega t + \theta_0) + V_0, \end{aligned} \quad (35)$$

which is a closed loop with a center at (δ_0, V_0) in the $\delta - V$ plane. Here, ω controls the varying speed of the Hamiltonian and the period is $T = 2\pi/\omega$. As in the discussions in the related studies [49,51], we would like to analyze the time-reversal symmetry of the model with the parameters given in Eq. (35). First, we rewrite the Hamiltonian in the form of Pauli operators, which is

$$\begin{aligned} H(t) = \sum_j \left[\frac{1 + (-1)^j \delta(t)}{2} c_j^\dagger \sigma^z c_{j+1} + \frac{\lambda i}{2} c_j^\dagger \sigma^y c_{j+1} + \text{H.c.} \right. \\ \left. + V(t) (-1)^{j+1} c_j^\dagger \sigma^z c_j \right], \end{aligned} \quad (36)$$

where the operator vector is given by $c_j^\dagger = (c_{j\uparrow}^\dagger, c_{j\downarrow}^\dagger)$, then we introduce the time-reversal operator defined as

$$\Theta = e^{-i\pi\sigma^y/2} K, \quad (37)$$

with K being the complex conjugation operator, and then we have

$$\Theta \sigma^\alpha \Theta^{-1} = -\sigma^\alpha \quad (38)$$

and

$$\Theta H(t) \Theta^{-1} \neq H(-t). \quad (39)$$

This means that $H(t)$ do not preserve the time-reversal symmetry due to Pauli matrix σ^z in the hopping term. This is a crucial difference from the two references.

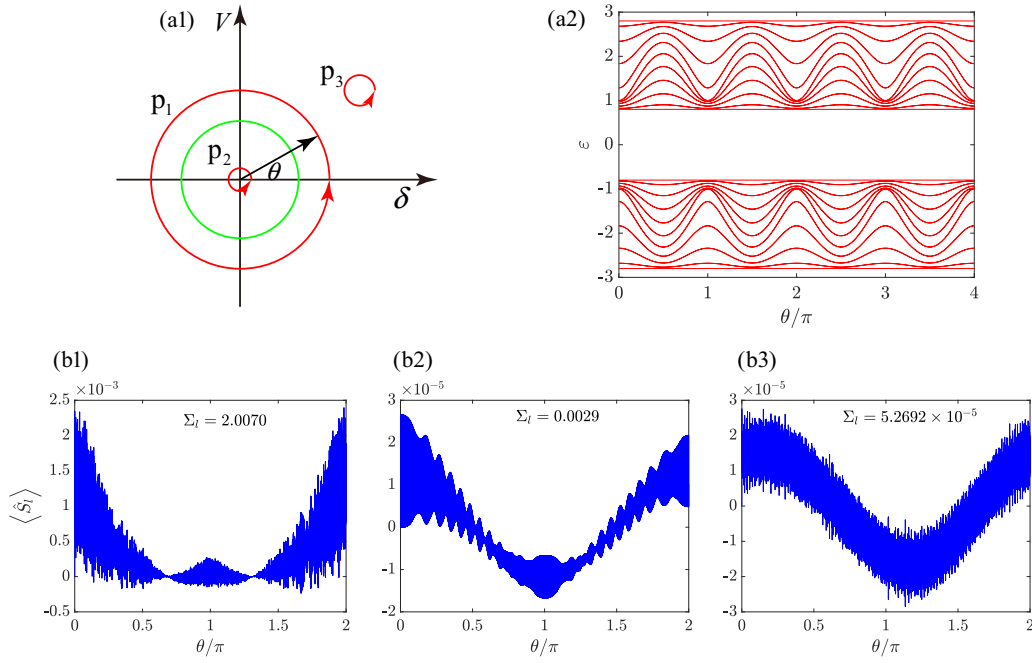


FIG. 2. Schematics of the adiabatic passages, the corresponding energy spectrum, pumping spin currents, and pumping spins of the ground state for several quasiadiabatic passages. The driven system adopts periodic boundary conditions to simulate the dynamic behavior of the topology originating from the nodal circles. (a1) The green circle represents the nodal circle for $\lambda = 1$ in the $\delta - V$ plane, while the red loops p_1 , p_2 , and p_3 are three adiabatic passages in parameter space with a counterclockwise direction. The corresponding parameter equations are as follows: p_1 : $\delta = 1.8 \cos(\omega t)$, $V = 1.8 \sin(\omega t)$; p_2 : $\delta = 0.05 \cos(\omega t)$, $V = 0.05 \sin(\omega t)$; p_3 : $\delta = 0.1 \cos(\omega t) + 2$, $V = 0.1 \sin(\omega t) + 2$. Panel (a2) shows the plot of the instantaneous spectrum of the time-dependent Hamiltonian for the passage p_1 , where $\theta = \omega t$ and the evolutionary period of every energy level is 2π . Panels (b1), (b2), and (b3) correspond to the spin currents $\langle \hat{S}_l \rangle = \langle \phi(t) | \hat{S}_l | \phi(t) \rangle$ and pumping spin Σ_l for the passages p_1 , p_2 , and p_3 , respectively, obtained from the numerical results for Eqs. (34) and (44). Here the position l is taken arbitrarily due to the translational symmetry. The results indicate that pumping spin is nearly quantized, being 2 or 0, determined by whether the adiabatic passage encircles the nodal circle or not. Other parameters are $N = 10$, $\omega = 0.001$, and $\Delta t = \pi/200$.

The pumping charge and spin for an evolution period can be expressed as

$$Q_{l,\sigma} = \int_0^T \langle \phi(t) | \hat{J}_{l,\sigma} | \phi(t) \rangle dt, \quad (40)$$

$$\Sigma_l = \int_0^T \langle \phi(t) | \hat{S}_l | \phi(t) \rangle dt, \quad (41)$$

where $|\phi(t)\rangle$ is the evolved state from the initial ground state $|\phi(0)\rangle$ of $H(0)$. The practical computation is performed by using a uniform mesh in time discretization. Time is discretized into t_m , with $t_0 = 0$ and $t_M = T$. For a given initial eigenstate $|\phi(0)\rangle$, the time-evolved state is computed using

$$|\phi(t_n)\rangle = \mathcal{T} \prod_{m=1}^n \exp[-iH(t_{m-1})(t_m - t_{m-1})] |\phi(0)\rangle, \quad (42)$$

where \mathcal{T} is the time-order operator. In the simulation, the value of M is considered sufficiently large to obtain a convergent result and the pumping charge and spin is

$$Q_{l,\sigma} \approx \sum_{m=1}^M \langle \phi(t_m) | \hat{J}_{l,\sigma} | \phi(t_m) \rangle \Delta t, \quad (43)$$

$$\Sigma_l \approx \sum_{m=1}^M \langle \phi(t_m) | \hat{S}_l | \phi(t_m) \rangle \Delta t, \quad (44)$$

where $\Delta t = (t_l - t_{l-1})$ is the time step. In the process of computation, the value of ω should be sufficiently small to fulfill the requirement of quasiadiabatic evolution.

In Fig. 2, the schematics of the adiabatic passages, the corresponding energy spectrum, pumping spin currents, and pumping spins of the ground state for several quasiadiabatic passages are presented. The results indicate that the pumping spin is nearly quantized, being 2 or 0, determined by whether the adiabatic passage encircles the nodal circle or not. The results are similar to the pumping charge of the ground state of a RM model with single degeneracy point, where the pumping charge is ± 1 or 0, determined by whether the adiabatic loop encircles the degenerate point or not. This strongly implies that the topology of the spinful RM model with spin-orbit coupling is the same as that in the single spinless RM model with a degenerate point. In addition, the pumping spin currents in Fig. 2(b) are approximately symmetric with respect to $\theta = \pi$ ($V = 0$), which probably originates from the symmetry described in Eq. (12).

VI. EDGE PUMPING SPIN FLIP

In the previous section, we explored the behavior of pumped spin under periodic boundary conditions. An intriguing question arises when considering open boundaries: what changes occur? A previous work has presented a method in terms of parallel transport and gauge fields to detect

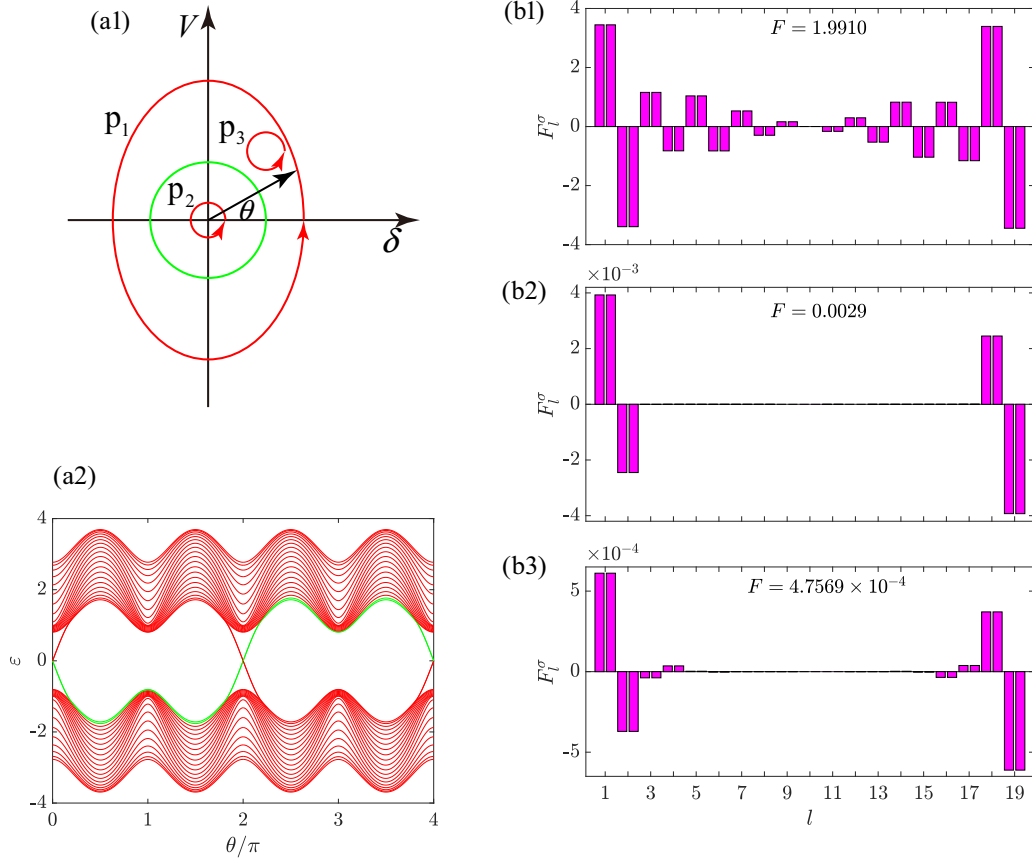


FIG. 3. Schematics of the adiabatic passages, the corresponding energy spectrum, pumping spin flip distribution, and total edge pumping spin flip of the ground state for several quasiadiabatic passages. The driven system adopts open boundary conditions to simulate the dynamic behavior of the boundary-bulk correspondence. (a1) The green circle represents the nodal circle for $\lambda = 1$ in the $\delta - V$ plane, while the red loops p_1 , p_2 , and p_3 are three adiabatic passages in parameter space with a counterclockwise direction. The corresponding parameter equations are as follows: p_1 : $\delta = 1.8 \cos(\omega t + \theta_0)$, $V = 2.7 \sin(\omega t + \theta_0)$; p_2 : $\delta = 0.05 \cos(\omega t + \theta_0)$, $V = 0.05 \sin(\omega t + \theta_0)$; p_3 : $\delta = 0.1 \cos(\omega t + \theta_0) + 1.3$, $V = 0.1 \sin(\omega t + \theta_0) + 1.3$. Panel (a2) shows the plot of the instantaneous spectrum of the time-dependent Hamiltonian for the passage p_1 , where $\theta = \omega t + \theta_0$ and the evolutionary period of every energy level is 4π . There is a crossing point between two energy levels of twofold degeneracy edge states at $\theta = 2\pi$. One of the edge energy levels is indicated in green. It indicates that any edge state completes its adiabatic cycle with a period of 4π . Panels (b1), (b2), and (b3) correspond to the distribution of the pumping spin flip F_l^σ and total edge pumping spin F for the passages p_1 , p_2 , and p_3 , respectively, obtained from the numerical results for Eqs. (47) and (48). We observe that the pumping spin flip F_l^σ vanishes in the bulk region. The results indicate that total edge pumping spin flip F is nearly quantized, being 2 or 0, determined by whether the adiabatic passage encircles the nodal circle or not. Other parameters are $N = 10$, $\omega = 0.0005$, $\theta_0 = \pi/2$, and $\Delta t = \pi/200$.

spin pumping current in an open system [53]. Inspired by this study, in the following, we focus on the system with open boundary conditions. In this situation, we always have $Q_\uparrow = Q_\downarrow = 0$ for any adiabatic passage due to the disconnection at the boundary. It is obvious that the total pumping spin is always zero for any adiabatic passage and thus cannot be used to characterize the topological feature. Nevertheless, we note that there should be an accumulation of particles at the ends of the chain, which may induce a spin-flip current. The operator of the spin-flip current can be defined as follows:

$$\mathcal{J}_l^\sigma = \frac{\lambda}{2i} c_{l,\sigma}^\dagger c_{l+1,-\sigma} + \text{H.c.}, \quad (45)$$

where $l \in [1, 2N - 1]$. In comparison with the normal current operator, it measures the current across sites l and $l + 1$, associated with spin flipping. When there is no spin-orbit coupling, it becomes clear that no spin flip current can flow, as the

channels remain disconnected. However, in the presence of spin-orbit coupling, a transport channel between two opposite spins exists, potentially creating an accumulation of spin flips. Similarly, we can define the pumped spin flip as

$$F_l^\sigma = \int_0^{2T} \langle \phi(t) | \mathcal{J}_l^\sigma | \phi(t) \rangle dt, \quad (46)$$

for a given adiabatic passage. Here, T is the period of the time-dependent Hamiltonian, with parameters as described in Eq. (35). In general, the integral period is T , corresponding to a single cycle of the quasiadiabatic time evolution along the adiabatic passage. However, for an open chain, a double cycle of the quasiadiabatic time evolution along the adiabatic passage should be considered to ensure that every initial single-particle eigenstate can evolve back. To demonstrate this point, we plot the energy level structure for the passage in Fig. 3(a2). We can observe that the edge states do not

revert after a single adiabatic passage cycle, whereas all other eigenstates do.

To perform numerical simulation of the quantity, we have

$$F_l^\sigma \approx \sum_{m=1}^{2M} \langle \phi(t_m) | \mathcal{J}_l^\sigma(t_m) | \phi(t_m) \rangle \Delta t, \quad (47)$$

which is similar to the formulation presented in Eq. (44). The details and the results are elucidated in Fig. 3. It displays several adiabatic loops in parameter space, while Fig. 3(a2) shows the energy spectrum of the adiabatic loop encircling the nodal circle in Fig. 3(a1). We find that two distinct energy levels, which are separated from the rest, correspond to the energies of the edge states. These two energy levels cross once after one period T , causing the edge state to adiabatically evolve along the green energy level depicted in Fig. 3(a2) and then return to its initial state after evolving for two periods. In (b1), (b2), and (b3) of Fig. 3 we present the corresponding simulation results for the pumping spin flip defined in Eq. (47). The results in Fig. 3(b1) demonstrate that $F_l^\sigma = F_l^{-\sigma}$, indicating that the pumping spin flip is position dependent. Specifically, the magnitude of the pumping spin flip decreases from the edges to the middle of the open chain, reaching zero at the center region. Furthermore, the pumping spin flip exhibits symmetry with respect to the center of the chain, but with opposite signs. To characterize the topology of the edge properties of the pumping spin flip, we introduce the concept of total pumping spin flip for a half chain, defined as follows:

$$F = \sum_{l=1, \sigma}^{N-1} F_l^\sigma, \quad (48)$$

which is the sum of the pumping spin flip over half of the sites. The numerical results reveal that the total pumping spin flip approaches the value of 2 with high precision when the adiabatic loop encircles the nodal circle. Conversely, when the adiabatic loop is either entirely within or outside the nodal circle, the total pumping spin flip is close to 0 with minimal deviation. Hence the quantized total pumping spin flip can serve as an indicator for the topology of the system under open boundary conditions. Here, it is worth noting that, although Fig. 3(b) indicates that the contribution of the pumping spin flip comes from the edge region, the contribution from the edge states is negligible. This suggests that the edge distribution of the pumping spin flip does not originate from the edge states. In addition, zero-energy edge states always exist for a given point inside the nodal loop. However, the corresponding evolved states do not exhibit chiral propagation. This result reveals the dynamic behavior associated with the boundary-bulk correspondence.

VII. SUMMARY

In summary, we investigate the dynamic demonstration on topology in association with nodal loop in a system with periodic and open boundary conditions. In contrast to the previous works, the nodal loop lies in a 2D parameter space, rather than a 3D space. The topology studied in the present work originates from a degenerate line, while in the previous work, such as that in Ref. [54], the related topology feature essentially

originates from an isolated degenerate point. Furthermore, we also investigate a dynamic manifestation of the boundary-bulk correspondence by computing the pumping spin flip for different adiabatic passages under the open boundary conditions. The results indicate that pumping spin flips at the edges are also quantized only for double periods of a closed passage. Our findings not only propose an origin for the topology but also provide another method for dynamically detecting the boundary-bulk correspondence.

ACKNOWLEDGMENT

This work was supported by the National Natural Science Foundation of China (under Grant No. 12374461).

DATA AVAILABILITY

No data were created or analyzed in this study.

APPENDIX A: NODAL LOOP

In this Appendix, we derive the equation for the nodal loop based on the spectrum provided in Eq. (25). When the energy gap closes, we obtain the following result:

$$(\zeta \zeta^* + \xi \xi^* + V^2)^2 = 4V^2 \xi \xi^* + (\zeta \xi^* + \xi \zeta^*)^2, \quad (A1)$$

which implies that

$$(\zeta \zeta^* - \xi \xi^* + V^2)^2 = (\zeta \xi^* - \xi \zeta^*)^2. \quad (A2)$$

Furthermore, by applying Eq. (24), we find that

$$\zeta \xi^* = \frac{\lambda}{2} [\delta(\cos k - 1) - i \sin k] \quad (A3)$$

and then

$$(\zeta \zeta^* - \xi \xi^* + V^2)^2 = -\lambda^2 \sin^2 k. \quad (A4)$$

Clearly, the equation has solutions only when k is either 0 or π . For $k = 0$, we get

$$\zeta \zeta^* - \xi \xi^* + V^2 = 1 + V^2 = 0, \quad (A5)$$

which indicates that there is no solution. For $k = \pi$, we get the solution

$$\delta^2 + V^2 = \lambda^2, \quad (A6)$$

which represents a circle with radius λ .

APPENDIX B: MAPPING TO A SEMIMETAL MODEL

At first, we map the core matrix h_k , given by Eq. (23) to a three-dimensional momentum space by replacing the parameters

$$(\delta, V, k) \rightarrow (-\gamma \sin k_x, \gamma \sin k_y, k_z + \pi), \quad (B1)$$

where $\gamma = \sqrt{1 - \lambda^2}/2$ ($|\lambda| < 1$). Note that such a map does not cover all the region of (δ, V) . However, we are only interested in the region in the vicinity of $(k_x, k_y, k_z) = (0, 0, 0)$. Second, in such a region, we have

$$\sin k_x \approx k_x, \quad \sin k_y \approx k_y. \quad (B2)$$

Then the matrix in Eq. (23) becomes

$$h_k \approx \tilde{h}_k = \gamma \begin{pmatrix} k_y & k_x + ik_z & \lambda/\gamma & 0 \\ k_x - ik_z & -k_y & 0 & \lambda/\gamma \\ \lambda/\gamma & 0 & k_y & k_x - ik_z \\ 0 & \lambda/\gamma & k_x + ik_z & -k_y \end{pmatrix}. \quad (\text{B3})$$

Third, applying a unitary transformation

$$U = \frac{1}{2} \begin{pmatrix} -i & 1 & i & 1 \\ 1 & -i & 1 & i \\ 1 & i & 1 & -i \\ i & 1 & -i & 1 \end{pmatrix}, \quad (\text{B4})$$

we find that

$$\tilde{h}_k \rightarrow \gamma \begin{pmatrix} k_z & k_x & 0 & \lambda/\gamma - k_y \\ k_x & -k_z & \lambda/\gamma + k_y & 0 \\ 0 & \lambda/\gamma + k_y & k_z & k_x \\ \lambda/\gamma - k_y & 0 & k_x & -k_z \end{pmatrix}, \quad (\text{B5})$$

which is identical to the matrix

$$H(\mathbf{q}) = \begin{pmatrix} q_z & q_x & 0 & -q_y + m \\ q_x & -q_z & q_y + m & 0 \\ 0 & q_y + m & q_z & q_x \\ -q_y + m & 0 & q_x & -q_z \end{pmatrix}, \quad (\text{B6})$$

appearing in Ref. [52]. As shown in this paper, this model describes a topological nodal line semimetal associated with the nodal ring

$$q_z = 0, \quad q_x^2 + q_y^2 = m^2, \quad (\text{B7})$$

in its spectrum

$$E(\mathbf{q}) = \pm \sqrt{q_z^2 + (\sqrt{q_x^2 + q_y^2} \pm m)^2}. \quad (\text{B8})$$

As reported in that work, a Z_2 invariant defined on a sphere enclosing the whole nodal loop is given for such a three-dimensional model.

-
- [1] D. J. Thouless, Quantization of particle transport, *Phys. Rev. B* **27**, 6083 (1983).
- [2] D. Xiao, M.-C. Chang, and Q. Niu, Berry phase effects on electronic properties, *Rev. Mod. Phys.* **82**, 1959 (2010).
- [3] M. Switkes, C. M. Marcus, K. Campman, and A. C. Gossard, An adiabatic quantum electron pump, *Science* **283**, 1905 (1999).
- [4] M. D. Blumenthal, B. Kaestner, L. Li, S. Giblin, T. J. B. M. Janssen, M. Pepper, D. Anderson, G. Jones, and D. A. Ritchie, Gigahertz quantized charge pumping, *Nat. Phys.* **3**, 343 (2007).
- [5] B. Kaestner, V. Kashcheyevs, S. Amakawa, M. D. Blumenthal, L. Li, T. J. B. M. Janssen, G. Hein, K. Pierz, T. Weimann, U. Siegner, and H. W. Schumacher, Single-parameter nonadiabatic quantized charge pumping, *Phys. Rev. B* **77**, 153301 (2008).
- [6] S. Nakajima, T. Tomita, S. Taie, T. Ichinose, H. Ozawa, L. Wang, M. Troyer, and Y. Takahashi, Topological Thouless pumping of ultracold fermions, *Nat. Phys.* **12**, 296 (2016).
- [7] M. Lohse, C. Schweizer, O. Zilberberg, M. Aidelsburger, and I. Bloch, A Thouless quantum pump with ultracold bosonic atoms in an optical superlattice, *Nat. Phys.* **12**, 350 (2016).
- [8] H.-I. Lu, M. Schemmer, L. M. Ayccock, D. Genkina, S. Sugawa, and I. B. Spielman, Geometrical pumping with a Bose-Einstein condensate, *Phys. Rev. Lett.* **116**, 200402 (2016).
- [9] J.-T. A. Chiang and Q. Niu, Quantum adiabatic particle transport in optical lattices, *Phys. Rev. A* **57**, R2278(R) (1998).
- [10] Y. Qian, M. Gong, and C. Zhang, Quantum transport of bosonic cold atoms in double-well optical lattices, *Phys. Rev. A* **84**, 013608 (2011).
- [11] L. Wang, M. Troyer, and X. Dai, Topological charge pumping in a one-dimensional optical lattice, *Phys. Rev. Lett.* **111**, 026802 (2013).
- [12] F. Matsuda, M. Tezuka, and N. Kawakami, Topological properties of ultracold bosons in one-dimensional quasiperiodic optical lattice, *J. Phys. Soc. Jpn.* **83**, 083707 (2014).
- [13] F. Mei, J.-B. You, D.-W. Zhang, X. C. Yang, R. Fazio, S.-L. Zhu, and L. C. Kwek, Topological insulator and particle pumping in a one-dimensional shaken optical lattice, *Phys. Rev. A* **90**, 063638 (2014).
- [14] R. Wei and E. J. Mueller, Anomalous charge pumping in a one-dimensional optical superlattice, *Phys. Rev. A* **92**, 013609 (2015).
- [15] Y.-B. Yang, L.-M. Duan, and Y. Xu, Continuously tunable topological pump in high-dimensional cold atomic gases, *Phys. Rev. B* **98**, 165128 (2018).
- [16] F. Matsuda, M. Tezuka, and N. Kawakami, Two-Dimensional Thouless pumping of ultracold fermions in obliquely introduced optical superlattice, *J. Phys. Soc. Jpn.* **89**, 114708 (2020).
- [17] Y. Zhang, Y. Gao, and D. Xiao, Topological charge pumping in twisted bilayer graphene, *Phys. Rev. B* **101**, 041410(R) (2020).
- [18] L. J. Geerligs, S. M. Verbrugh, P. Hadley, J. E. Mooij, H. Pothier, P. Lafarge, C. Urbina, D. Estève, and M. H. Devoret, Single Cooper pair pump, *Z. Phys. B* **85**, 349 (1991).
- [19] J. P. Pekola, J. J. Toppari, M. Aunola, M. T. Savolainen, and D. V. Averin, Adiabatic transport of Cooper pairs in arrays of Josephson junctions, *Phys. Rev. B* **60**, R9931 (1999).
- [20] R. Fazio, F. W. J. Hekking, and J. P. Pekola, Measurement of coherent charge transfer in an adiabatic Cooper-pair pump, *Phys. Rev. B* **68**, 054510 (2003).
- [21] R. Leone, L. P. Lévy, and P. Lafarge, Cooper-pair pump as a quantized current source, *Phys. Rev. Lett.* **100**, 117001 (2008).
- [22] R.-P. Riwar, M. Houzet, J. S. Meyer, and Y. V. Nazarov, Multi-terminal Josephson junctions as topological matter, *Nat. Commun.* **7**, 11167 (2016).
- [23] H.-Y. Xie, M. G. Vavilov, and A. Levchenko, Weyl nodes in Andreev spectra of multiterminal Josephson junctions: Chern numbers, conductances, and supercurrents, *Phys. Rev. B* **97**, 035443 (2018).
- [24] J. C. Y. Teo and C. L. Kane, Topological defects and gapless modes in insulators and superconductors, *Phys. Rev. B* **82**, 115120 (2010).

- [25] A. Keselman, L. Fu, A. Stern, and E. Berg, Inducing time reversal-invariant topological superconductivity and fermion parity pumping in quantum wires, *Phys. Rev. Lett.* **111**, 116402 (2013).
- [26] P. Kotetes, M. T. Mercaldo, and M. Cuoco, Synthetic Weyl points and chiral anomaly in Majorana devices with nonstandard Andreev-bound-state spectra, *Phys. Rev. Lett.* **123**, 126802 (2019).
- [27] M. Houzet and J. S. Meyer, Majorana-Weyl crossings in topological multiterminal junctions, *Phys. Rev. B* **100**, 014521 (2019).
- [28] M. T. Mercaldo, P. Kotetes, and M. Cuoco, Magnetoelectrically-tunable Andreev-bound-state spectra and spin polarization in P-wave Josephson junctions, *Phys. Rev. B* **100**, 04519 (2019).
- [29] A. A. Burkov, M. D. Hook, and L. Balents, Topological nodal semimetals, *Phys. Rev. B* **84**, 235126 (2011).
- [30] J.-M. Carter, V. V. Shankar, M. A. Zeb, and H.-Y. Kee, Semimetal and topological insulator in perovskite iridates, *Phys. Rev. B* **85**, 115105 (2012).
- [31] W. B. Rui, Y. X. Zhao, and A. P. Schnyder, Topological transport in Dirac nodal-line semimetals, *Phys. Rev. B* **97**, 161113(R) (2018).
- [32] C. Chen, X. T. Zeng, Z. Chen, Y. X. Zhao, X. L. Sheng, and S. A. Yang, Second-order real nodal-line semimetal in three-dimensional graphdiyne, *Phys. Rev. Lett.* **128**, 026405 (2022).
- [33] L. Li, J. Cao, C. Cui, Z.-M. Yu, and Y. Yao, Planar Hall effect in topological Weyl and nodal-line semimetals, *Phys. Rev. B* **108**, 085120 (2023).
- [34] G. Bian, T.-R. Chang, R. Sankar, S.-Y. Xu, H. Zheng, T. Neupert, C.-K. Chiu, S.-M. Huang, G. Chang, I. Belopolski, D. S. Sanchez, M. Neupane, N. Alidoust, C. Liu, B. Wang, C.-C. Lee, H.-T. Jeng, C. Zhang, Z. Yuan, S. Jia *et al.*, Topological nodal-line fermions in spin-orbit metal PbTaSe₂, *Nat. Commun.* **7**, 10556 (2016).
- [35] C. Chen, X. Xu, J. Jiang, S.-C. Wu, Y. P. Qi, L. X. Yang, M. X. Wang, Y. Sun, N. B. M. Schröter, H. F. Yang *et al.*, Dirac line nodes and effect of spin-orbit coupling in the nonsymmorphic critical semimetals $MSiS$ ($M = \text{Hf, Zr}$), *Phys. Rev. B* **95**, 125126 (2017).
- [36] Y. Du, X. Bo, D. Wang, E.-J. Kan, C.-G. Duan, S. Y. Savrasov, and X. Wan, Emergence of topological nodal lines and type-II Weyl nodes in the strong spin-orbit coupling system InNbX_2 ($X = \text{S, Se}$), *Phys. Rev. B* **96**, 235152 (2017).
- [37] D. F. Liu, E. K. Liu, Q. N. Xu, J. L. Shen, Y. W. Li, D. Pei, A. J. Liang, P. Dudin, T. K. Kim, C. Cacho, Y. F. Xu, Y. Sun, L. X. Yang, Z. K. Liu, C. Felser, S. S. P. Parkin, and Y. L. Chen, Direct observation of the spin-orbit coupling effect in magnetic Weyl semimetal $\text{Co}_3\text{Sn}_2\text{S}_2$, *npj Quantum Mater.* **7**, 11 (2022).
- [38] F. Zhou, Topological spin pumps: The effect of spin rotation on quantum pumps, *Phys. Rev. B* **70**, 125321 (2004).
- [39] V. Brosco, M. Jerger, P. San-José, G. Zarand, A. Shnirman, and G. Schön, Prediction of resonant all-electric spin pumping with spin-orbit coupling, *Phys. Rev. B* **82**, 041309(R) (2010).
- [40] K. Chen and S. Zhang, Spin pumping in the presence of spin-orbit coupling, *Phys. Rev. Lett.* **114**, 126602 (2015).
- [41] M. Yama, M. Tatsuno, T. Kato, and M. Matsuo, Spin pumping of two-dimensional electron gas with Rashba and Dresselhaus spin-orbit interactions, *Phys. Rev. B* **104**, 054410 (2021).
- [42] E. H. Fyhn and J. Linder, Spin-orbit pumping, *Phys. Rev. B* **105**, L020409 (2022).
- [43] O. Ly and A. Manchon, Spin-orbit coupling induced ultrahigh-harmonic generation from magnetic dynamics, *Phys. Rev. B* **105**, L180415 (2022).
- [44] C. Sun and J. Linder, Spin pumping from a ferromagnetic insulator into an altermagnet, *Phys. Rev. B* **108**, L140408 (2023).
- [45] M. Yama, M. Matsuo, and T. Kato, Effect of vertex corrections on the enhancement of Gilbert damping in spin pumping into a two-dimensional electron gas, *Phys. Rev. B* **107**, 174414 (2023).
- [46] C. Schweizer, M. Lohse, R. Citro, and I. Bloch, Spin pumping and measurement of spin currents in optical superlattices, *Phys. Rev. Lett.* **117**, 170405 (2016).
- [47] K.-R. Jeon, C. Ciccarelli, H. Kurebayashi, L. F. Cohen, X. Montiel, M. Eschrig, S. Komori, J. W. A. Robinson, and M. G. Blamire, Exchange-field enhancement of superconducting spin pumping, *Phys. Rev. B* **99**, 024507 (2019).
- [48] Y. Li, W. Cao, V. P. Amin, Z. Zhang, J. Gibbons, J. Sklenar, J. Pearson, P. M. Haney, M. D. Stiles, W. E. Bailey, V. Novosad, A. Hoffmann, and W. Zhang, Coherent spin pumping in a strongly coupled magnon-magnon hybrid system, *Phys. Rev. Lett.* **124**, 117202 (2020).
- [49] L. Fu and C. L. Kane, Time reversal polarization and a Z_2 adiabatic spin pump, *Phys. Rev. B* **74**, 195312 (2006).
- [50] E. Prodan, Robustness of the spin-Chern number, *Phys. Rev. B* **80**, 125327 (2009).
- [51] C. Q. Zhou, Y. F. Zhang, L. Sheng, R. Shen, D. N. Sheng, and D. Y. Xing, Proposal for a topological spin Chern pump, *Phys. Rev. B* **90**, 085133 (2014).
- [52] C. Fang, Y. Chen, H.-Y. Kee, and L. Fu, Topological nodal line semimetals with and without spin-orbital coupling, *Phys. Rev. B* **92**, 081201(R) (2015).
- [53] H.-Q. Zhou, S. Y. Cho, and R. H. McKenzie, Gauge fields, geometric phases, and quantum adiabatic pumps, *Phys. Rev. Lett.* **91**, 186803 (2003).
- [54] R. Wang, C. Li, X. Z. Zhang, and Z. Song, Dynamical bulk-edge correspondence for degeneracy lines in parameter space, *Phys. Rev. B* **98**, 014303 (2018).